

Effects of grain-boundary configuration on the high-temperature creep strength of cobalt-base L-605 alloys

M. TANAKA, H. IIZUKA, M. TAGAMI*

*Department of Mechanical Engineering for Production, and *Department of Metallurgy, Mining College, Akita University, 1-1 Tegatagakuen-cho, Akita 010, Japan*

The effects of grain-boundary configuration on the high-temperature creep strength are investigated using commercial cobalt-base L-605 alloys with low carbon content in the temperature range 816 to 1038°C (1500 to 1900°F). Serrated grain boundaries are formed principally by the precipitation of tungsten-rich bcc phase (the same as α_2 phase found in Ni-20Cr-20W alloys) on grain boundaries by a relatively simple heat treatment in these alloys. The creep rupture properties are improved by strengthening of grain boundaries by the precipitation of tungsten-rich bcc (α_2) phase. The specimens with serrated grain boundaries have longer rupture lives and higher ductility than those with normal straight grain boundaries under low stress and high-temperature creep conditions, while the rupture lives and the creep ductility of both specimens are almost the same under high stresses below 927°C. The matrix of the alloys is strengthened by the precipitation of carbides at temperatures below 927°C and by the precipitation of tungsten-rich α_2 phase at 1038°C during creep. It is found that there is an orientation relationship between tungsten-rich α_2 phase particles and β -Co matrix, such that $(011)_{\alpha_2} \parallel (111)_{\beta\text{-Co}}$ and $[1\bar{1}1]_{\alpha_2} \parallel [1\bar{1}0]_{\beta\text{-Co}}$. The fracture surface of specimens with serrated grain boundaries is a ductile grain-boundary fracture surface, while typical grain-boundary facets prevailed in specimens with straight grain boundaries.

1. Introduction

It has been reported by many investigators that serrated grain boundaries are effective in improving the high-temperature strength of polycrystalline heat-resisting alloys [1-5]. The effectiveness of grain-boundary strengthening by serrated grain boundaries is also confirmed in cobalt-base HS-21 superalloys with high carbon contents at 816°C (1500°F) [6, 7]. However, it is not easy in low carbon heat-resistant alloys to obtain serrated grain boundaries by heat treatment [8]. It is also believed that the creep rupture strength is not improved by serrated grain boundaries without concomitant matrix hardening by precipitates [3].

In this study, the occurrence of serrated grain boundaries is at first examined on cobalt-base L-605 superalloys with low carbon content (0.07 wt % C) by heat treatment. The effect of serrated grain boundaries on the creep rupture strength is then investigated using the same alloys in the temperature range from 816 to 1038°C (1500 to 1900°F). The effectiveness of serrated grain boundaries is discussed based on the relationship between creep rupture strength and microstructures in these alloys.

2. Experimental procedure

Table I shows the chemical composition of cobalt-base L-605 alloy bars of 20 mm diameter used in this

study. This kind of alloy contains a relatively small amount of carbon compared with the other class of cobalt-base alloys such as HS-21 alloys [9]. Therefore, the experiments were at first made to identify the heat treatment to cause serrated grain boundaries in these alloys. The heat-treated specimens were machined to test pieces of 6 mm diameter and 30 mm gauge length for creep rupture experiments.

Creep rupture experiments were performed using these specimens in the temperature range from 816 to 1038°C (1500 to 1900°F) in air. The specimens were aged for 3 h at each test temperature and were then loaded. The microstructure and fracture appearance of ruptured specimens were examined using both optical and scanning electron microscopes. Specimens were electrolytically etched by 10% chromic acid in water before observations by optical microscopy. A transmission electron microscope was employed to identify the grain-boundary precipitates in these specimens. In addition, elements dissolved in the precipitates were examined by an electron probe microanalyser (EPMA).

TABLE I Chemical composition of cobalt-base L-605 alloys used (wt %)

Alloy	C	Cr	Ni	W	Mn	Fe	Si	P	S	Co
L-605	0.07	19.82	9.83	14.37	1.46	2.22	0.19	<0.005	0.002	bal.

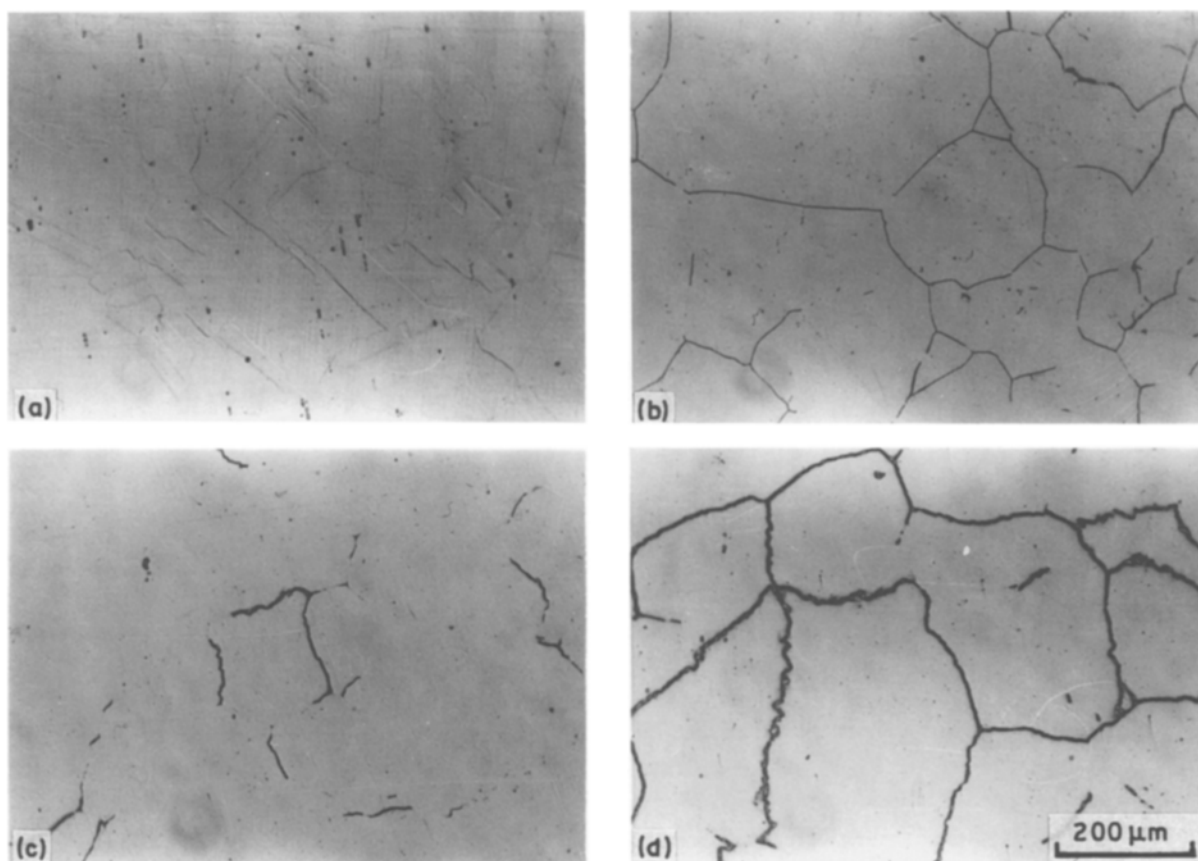


Figure 1 Microstructures of heat-treated specimens. (a) 1200°C 2 h → WQ (alloy N). (b) 1200°C 2 h → FC. (c) 1200°C 1 h (FC) → 1050°C 5 h → WQ. (d) 1200°C 1 h (FC) → 1050°C 20 h → WQ (alloy S). WQ = water quenched, FC = furnace cooled.

3. Results and discussion

3.1. Effects of heat treatment on the grain-boundary configuration

Fig. 1 shows microstructures of heat-treated specimens. The grain boundary is straight and no precipitates are observed in the water-quenched specimen after solution treatment for 2 h at 1200°C (Fig. 1a). This specimen is described as “specimen with straight grain boundaries” or simply “alloy N” in this study. Grain-boundary precipitates are detectable in the furnace-cooled specimen after the same solution treatment as the water-quenched specimen, but the grain boundaries are not serrated so much (Fig. 1b). Figs 1c and d are microstructures of specimens furnace-cooled to 1050°C after solution treatment for 1 h at 1200°C and held for 5 and 20 h at this temperature and then water-quenched, respectively. The grain boundaries of these specimens are considerably serrated by nucleation and growth of the grain-boundary precipitates in the grain-growth process during holding at 1050°C. It is confirmed that holding for 20 h at 1050°C is sufficient almost completely to develop serrated grain boundaries, while grain boundaries are partly serrated by 5 h holding at the same temperature. The former specimen is termed “specimen with serrated grain boundaries” or simply “alloy S” in this study. No matrix precipitates are observed on these specimens. Both specimens with serrated grain boundaries (alloy S) and those with normal straight grain boundaries (alloy N) have almost the same grain size (260 μm) and the same initial matrix hardness (250 Hv).

Fig. 2 shows the transmission electron micrographs

of alloys S and N. No precipitates are observed on alloy N with straight grain boundaries (Fig. 2a), but large precipitates are visible on grain boundaries in alloy S (Fig. 2b). The diffraction pattern of Fig. 2b (Fig. 2c) indicates that these precipitates are the same as tungsten-rich α_2 phase with body-centred cubic (bcc) structure in Ni-20Cr-20W alloys [10]. Therefore, this phase is referred to as α_2 phase in this paper. It is found in this study that the close-packed plane of tungsten-rich bcc phase (α_2 phase) is parallel to that of β -Co matrix (face-centred cubic, fcc), and that the orientation relationship is such that $(011)_{\alpha_2} \parallel (111)_{\beta\text{-Co}}$ and $[1\bar{1}1]_{\alpha_2} \parallel [1\bar{1}0]_{\beta\text{-Co}}$.

Fig. 3 shows the results of line analysis on elements dissolved in grain-boundary precipitates in alloy S by an electron probe microanalyser (EPMA). Grain-boundary precipitates (white areas) are observed in the scanning electron micrograph (Fig. 3a), and are very rich in tungsten (W) and depleted in both chromium (Cr) and cobalt (Co) (Fig. 3c). These are tungsten-rich α_2 phase which are identified by electron diffraction of thin foils (Fig. 2c). Other grain-boundary precipitates in the grey areas which are much smaller in size than, and are adjacent to, the α_2 phase (white precipitates) (Fig. 3b) are rich in both chromium (Cr) and tungsten (W) and rather poor in cobalt (Co). As reported by Yukawa and Sato [11], these precipitates are probably M_6C -type carbides, because this type of carbide can dissolve larger amounts of tungsten than $M_{23}C_6$ -type carbides [12, 13].

As pointed out by Tu and Turnbull [14], grain-boundary precipitates are nucleated so as to minimize

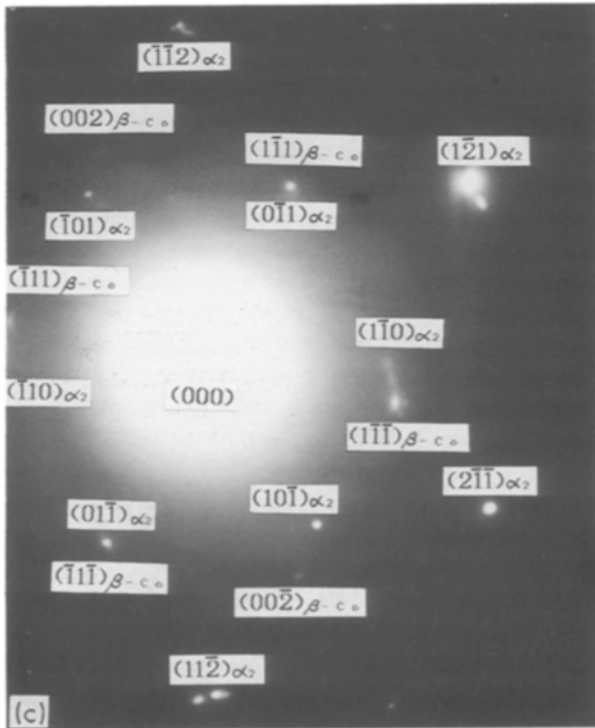


Figure 2 The electron transmission micrographs of L-605 alloys. (a) Alloy N; (b) alloy S; (c) selected-area electron diffraction pattern of (b) $((001)_{\alpha_2} \parallel (111)_{\beta-Co}, [1\bar{1}1]_{\alpha_2} \parallel [1\bar{1}0]_{\beta-Co})$.

3.2. Effects of grain-boundary configuration on creep rupture properties

Fig. 4 shows the rupture lives of L-605 alloys at high temperatures. The rupture lives of specimens with serrated grain boundaries (alloy S) are longer than those of specimens with straight grain boundaries (alloy N) under low-stress and high-temperature creep conditions, while the creep rupture strength of alloy S is almost the same as that of alloy N under high stresses below 927°C. For example, the rupture life of alloy S is about 344 h and that of alloy N is about 174 h under a stress of 58.8 MPa at 927°C. Fig. 5 shows the creep ductility of L-605 alloys at high temperatures. The creep ductility of specimens with serrated grain boundaries is larger than that of specimens with straight grain boundaries under low stress and high-temperature conditions, but it is almost the same in both specimens under high stresses below 927°C.

Fig. 6 shows examples of creep curves in L-605 alloys. L-605 alloys show normal creep curves with transient, steady-state, and accelerated creep terms, irrespective of grain-boundary configuration in the temperature range from 816 to 1038°C. Fig. 7 shows the relation between steady-state creep rate and stress in L-605 alloys. The stress dependence of steady-state creep rate is almost the same in alloy S and alloy N in the temperature range from 816 to 1038°C, and the stress exponent is about 8 when a power law ($\dot{\epsilon}_s \propto \sigma^n$, $\dot{\epsilon}_s$ is the steady-state creep rate, σ the stress, n the stress exponent) is applied. The strength of grains seems to be almost the same in both specimens under the same creep conditions, because there is little difference between the steady-state creep rate of alloy S and that of alloy N under all creep conditions.

the surface energy by lying on either habit plane of two adjacent grains in the early stage of grain-boundary reaction during ageing, and serrated grain boundaries are formed as a result. In some cases, there is some fixed orientation relationship between the second phase and the matrix, such as $M_{23}C_6$ carbides and austenite matrix in 21Cr-4Ni-9Mn steels [15], $M_{23}C_6$ carbides and β -Co matrix in cobalt-base HS-21 alloys [6], and tungsten-rich α_2 phase and β -Co matrix in cobalt-base L-605 alloys in this study. Therefore, it is concluded that serrated grain boundaries can be obtained by a simple heat treatment if there is some orientation relationship between second phase and matrix phase.

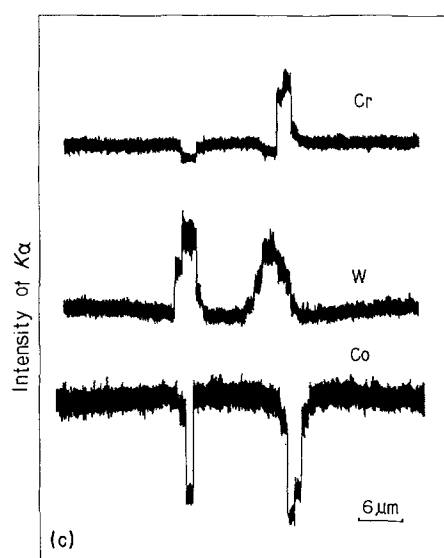
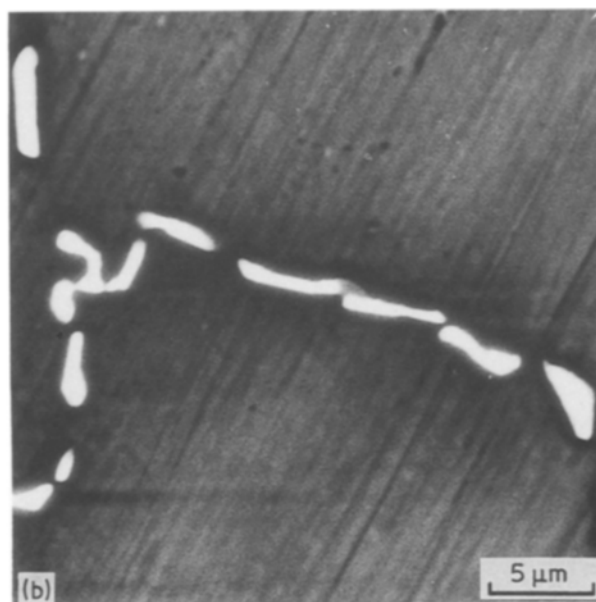
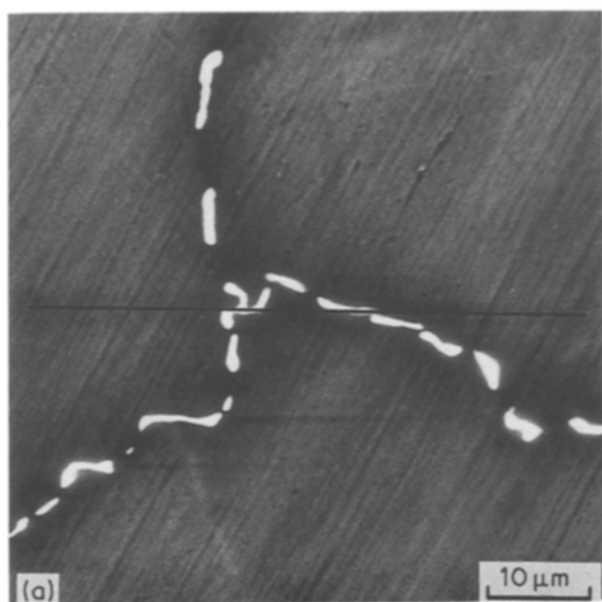


Figure 3 The results of line analysis on elements dissolved in grain-boundary precipitates in alloy S by EPMA. (a) Scanning electron micrograph. (b) Enlarged photograph of (a). (c) Profile of elements by line analysis.

3.3. Microstructures and fracture appearance of ruptured specimens

Fig. 8 shows the microstructure and fracture surface of the specimen with serrated grain boundaries (alloy S) and that with straight grain boundaries (alloy N) ruptured under a stress of 118 MPa at 816°C. The tensile direction is horizontal in optical micrographs. Grain-boundary cracks can be observed especially at grain-boundary triple junctions near the fracture surface of the specimens (Figs 8a and b). Fine dispersions of matrix precipitates are formed on both the specimens, and very small grain-boundary precipitates are nucleated on straight grain boundaries of alloy N. The grains are largely elongated in the tensile direction in both specimens. The fracture surface of alloy S consists of steps and ledges which correspond to facets of serrated grain boundaries, and small dimples are also visible on the fracture surface of this specimen (Fig. 8c). The fracture surface of alloy N is featureless and

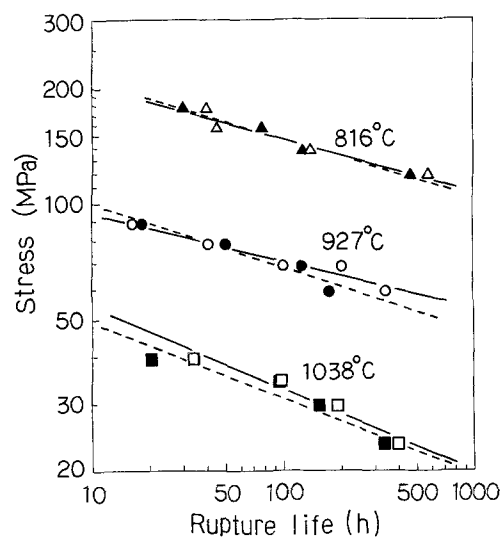


Figure 4 The rupture lives of L-605 alloys at high temperatures. (Δ , \circ , \square) Alloy S, (\blacktriangle , \bullet , \blacksquare) alloy N. Temperature ($^{\circ}\text{C}$): (Δ , \blacktriangle) 816, (\circ , \bullet) 927, (\square , \blacksquare) 1038.

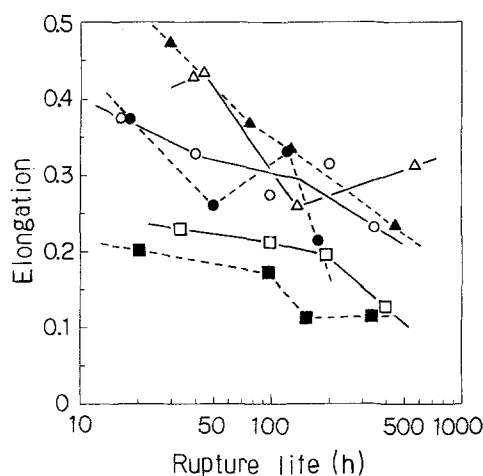


Figure 5 The creep ductility of L-605 alloys at high temperatures. (Δ , \circ , \square) Alloy S, (\blacktriangle , \bullet , \blacksquare) alloy N. Temperature ($^{\circ}\text{C}$): (Δ , \blacktriangle) 816, (\circ , \bullet) 927, (\square , \blacksquare) 1038.

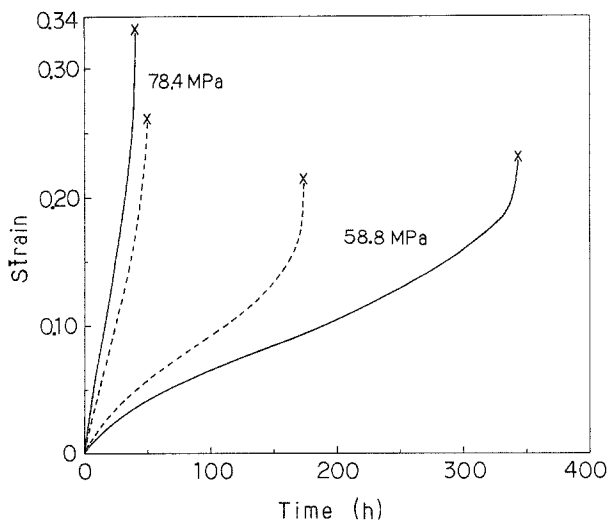


Figure 6 Examples of creep curves in L-605 alloys at 927°C. (—) Alloy S, (---) alloy N.

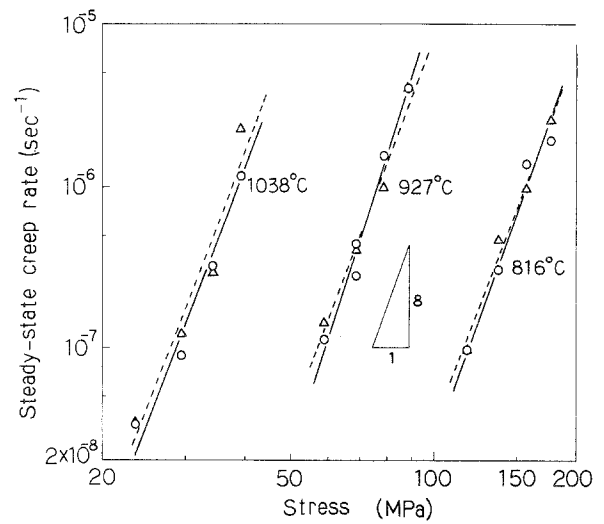


Figure 7 Stress dependence of steady-state creep rate in L-605 alloys. (O) Alloy S, (Δ) alloy N.

smooth grain-boundary facets (Fig. 8d). Fig. 9 shows the microstructure and fracture surface of specimens ruptured under a stress of 29.4 MPa at 1038°C. Many microcracks can be observed on grain boundaries and large precipitates are visible both in the matrix and on the grain boundaries of both specimens (Figs 9a and b). The recrystallization can be also observed near the fracture surface of both specimens. The fracture surface of alloy S consists of ledges and fine dimples similar to those found in Fig. 8c. The fracture surface of alloy N is principally grain-boundary facets, but fine dimples are also found in the specimen at this temperature.

Fig. 10 shows subgrains observed on the ruptured specimens. Elongated small subgrains and many precipitates are formed within grains in alloy N at 816°C (Fig. 10a), while equiaxed subgrains are formed in alloy S at 1038°C (Fig. 10b). Fig. 11 shows the results of line analysis on elements dissolved in grain-boundary and matrix precipitates in alloy N ruptured under a stress of 118 MPa at 816°C. Most of grain-boundary precipitates and matrix precipitates are rich in both chromium (Cr) and tungsten (W), and are depleted in cobalt (Co). Thus, these precipitates are probably M_6C -type carbides [12, 13]. Similar results of line analysis are obtained on the matrix precipitates in

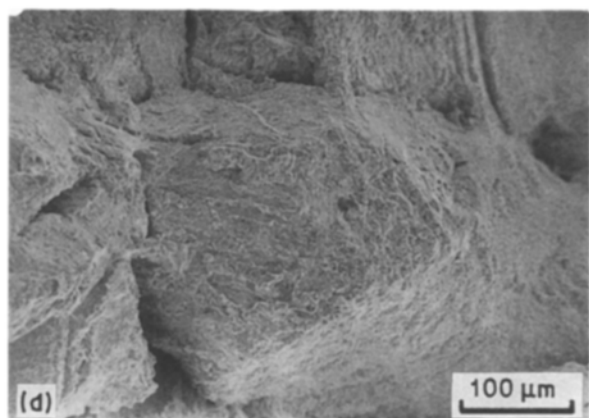
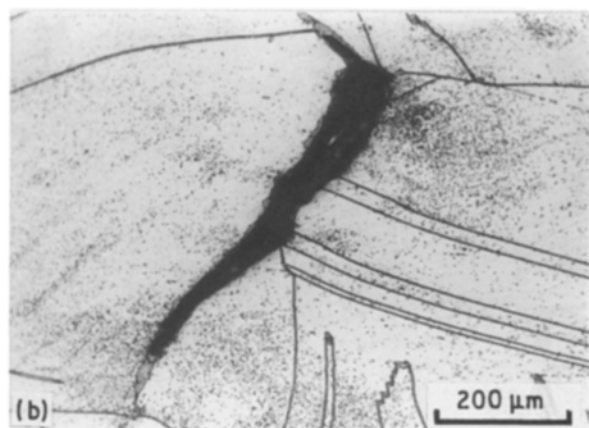
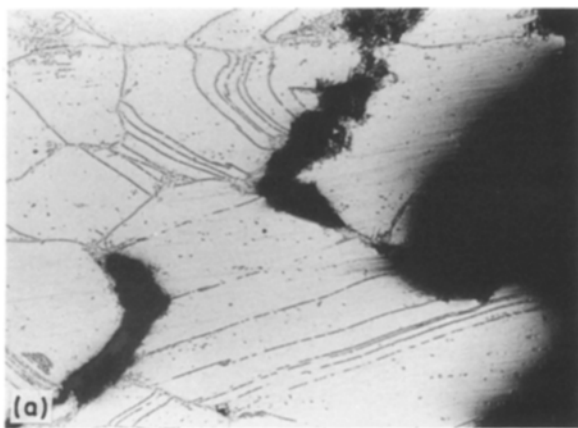


Figure 8 The microstructure and fracture surface of specimens ruptured under a stress of 118 MPa at 816°C. (a), (c) Alloy S, (b), (d) alloy N.

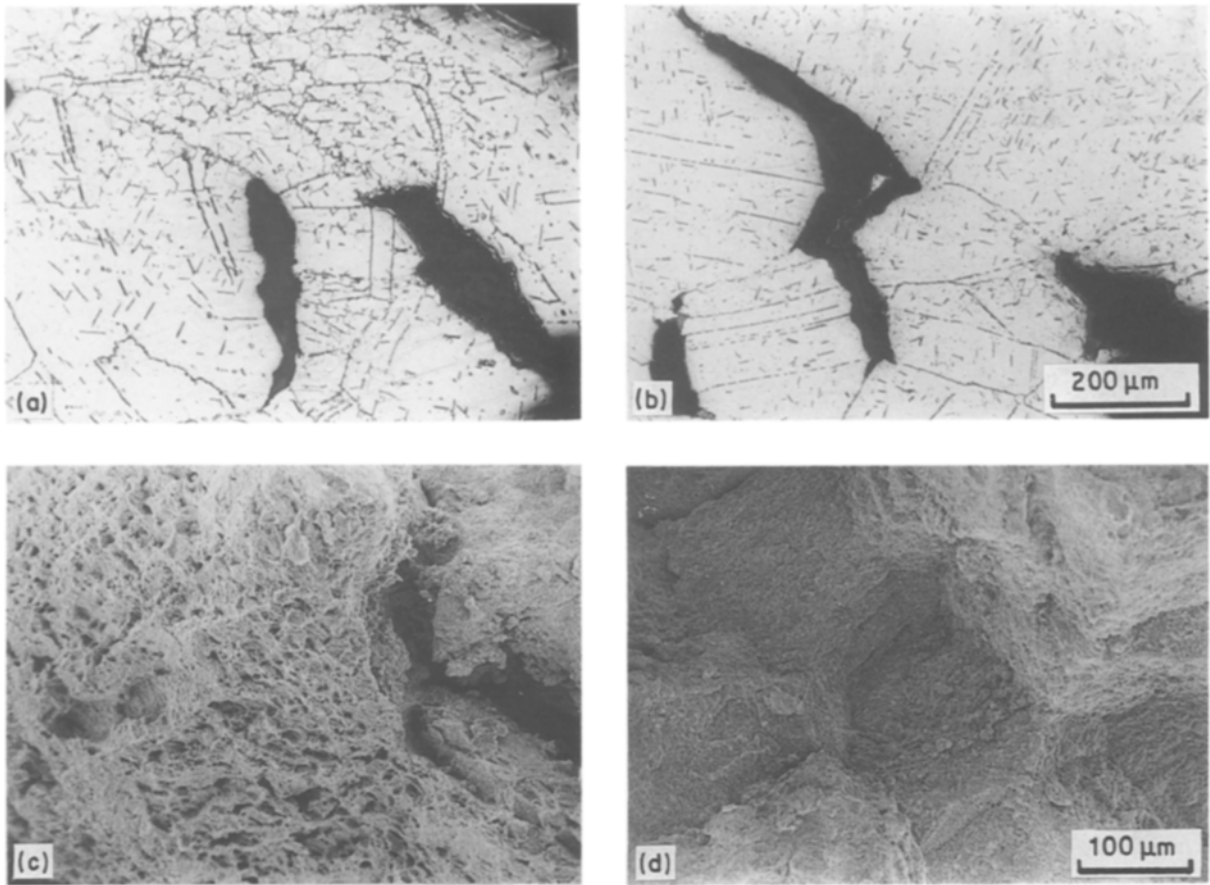


Figure 9 The microstructure and fracture surface of specimens ruptured under a stress of 29.4 MPa at 1038°C. (a), (c) Alloy S; (b), (d) alloy N.

alloy S ruptured under the same conditions, while grain-boundary M_6C carbides tend to be formed adjacent to grain-boundary α_2 phase in this specimen (Fig. 3).

Fig. 12 shows the results of line analysis on elements dissolved in grain-boundary and matrix precipitates in

alloy N ruptured under a stress of 29.4 MPa at 1038°C. Continuous grain-boundary precipitates which were formed during creep are mostly tungsten-rich bcc phase (α_2 phase) in alloy N as well as alloy S at this temperature (Fig. 12a). Widmannstätten precipitates in the matrix are α_2 phase (Fig. 12b), and are also

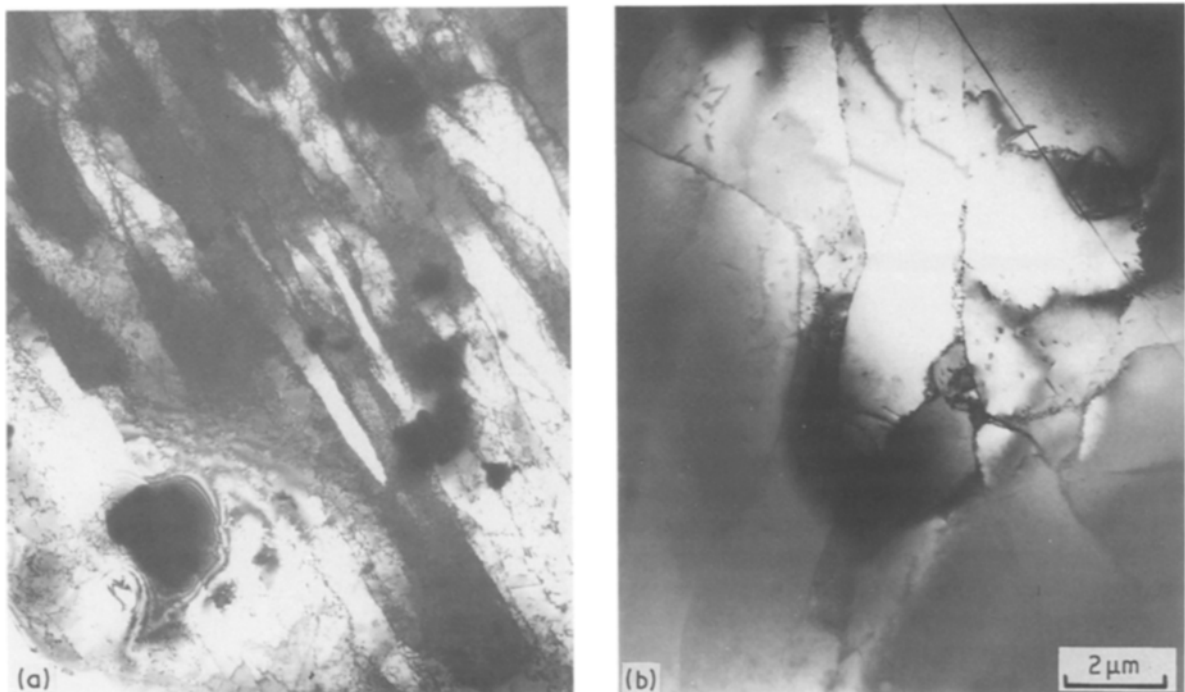


Figure 10 Subgrains observed on the ruptured specimens. (a) Alloy N ruptured under a stress of 118 MPa at 816°C, (b) alloy S ruptured under a stress of 29.4 MPa at 1038°C.

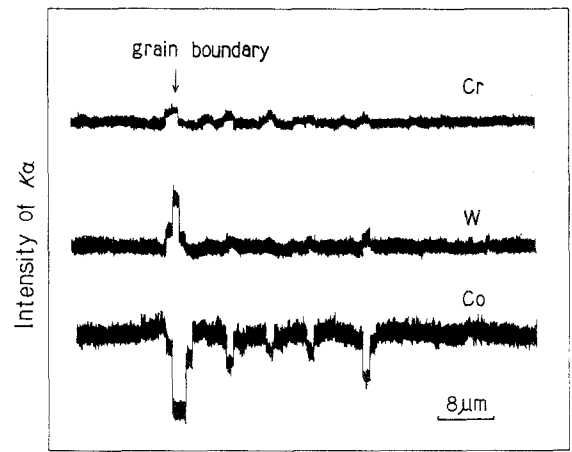
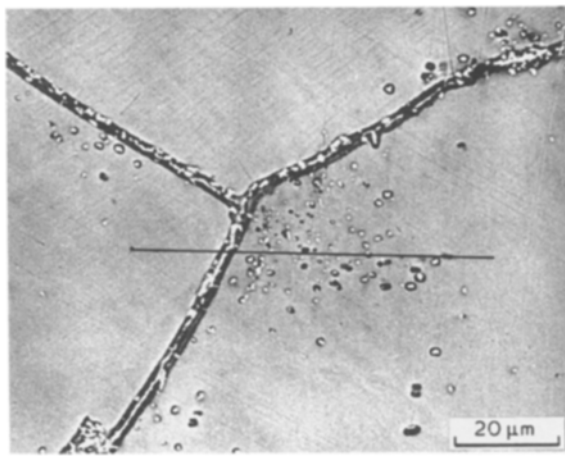


Figure 11 The results of line analysis on elements dissolved in grain-boundary and matrix precipitates in alloy N ruptured under a stress of 118 MPa at 816°C, by EPMA.

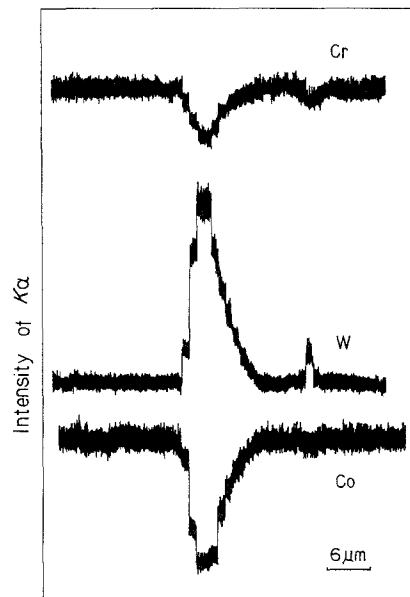
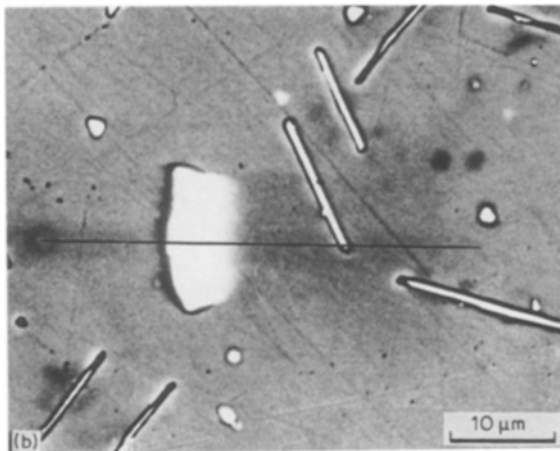
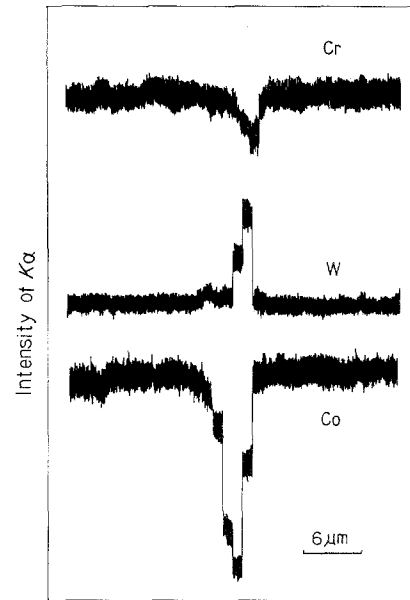
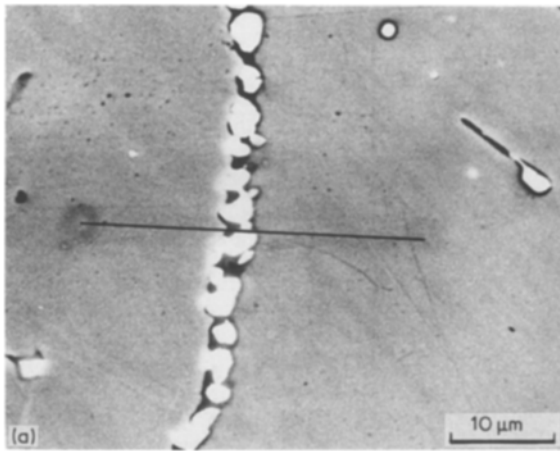


Figure 12 The results of line analysis on elements dissolved in grain-boundary and matrix precipitates in alloy N ruptured under a stress of 29.4 MPa at 1038°C, by EPMA. (a) Grain-boundary precipitate (α_2 phase); (b) matrix precipitate (α_2 phase).

observed in the matrix of alloy S ruptured under the same creep conditions. These α_2 phase in the matrix are plate-like or rod-like in form and have the same orientation relationship with β -Co matrix (fcc) as grain-boundary α_2 phase (alloy S).

In addition to these precipitates, small amounts of Laves phase and $M_{23}C_6$ -type carbides are also detected by electron diffraction of thin films. Laves phase is observed on grain boundaries of alloys S and N during creep at 816°C, while $M_{23}C_6$ carbides are formed principally in rectangular shape in the matrix of the specimens [11]. However, we consider in this study that L-605 alloys are strengthened by serrated grain boundaries principally with tungsten-rich α_2 phase and by M_6C and $M_{23}C_6$ carbides in the matrix at temperatures around 816°C, while the strengthening of the alloys is related to the precipitation of α_2 phase both on grain boundaries and in the matrix at 1038°C.

4. Conclusions

The effect of strengthening by serrated grain boundaries on the creep rupture properties was investigated using cobalt-base L-605 alloys with low carbon contents in the temperature range from 816 to 1038°C (1500 to 1900°F). The results obtained are summarized below.

1. The creep rupture strength was improved by serrated grain boundaries. The rupture lives of specimens with serrated grain boundaries were longer than that of specimens with normal straight grain boundaries under low stress and high-temperature conditions, while the rupture lives of both specimens were almost the same under high stresses below 927°C. The creep ductility was also improved by serrated grain boundaries under low-stress and high-temperature conditions.

2. The serrated grain boundaries were formed as a result of precipitation of tungsten-rich α_2 phase on grain boundaries by a heat treatment. Thus, the grain-boundary strengthening in specimens with serrated grain boundaries was principally due to the formation of α_2 phase. The α_2 phase particles were formed also in the matrix of specimens with serrated grain boundaries and those with straight grain boundaries during creep at 1038°C, and contributed to the strengthening of the matrix. There was an orientation relation-

ship between α_2 phase and β -Co matrix, such that $(011)_{\alpha_2} \parallel (111)_{\beta\text{-Co}}$ and $[\bar{1}\bar{1}1]_{\alpha_2} \parallel [1\bar{1}0]_{\beta\text{-Co}}$. M_6C and $M_{23}C_6$ carbides^{Co} were probably the strengthening phases of the matrix at temperatures around 816°C.

3. The fracture surface of specimens with serrated grain boundaries was a ductile grain-boundary fracture surface which consisted of steps and ledges corresponding to serrated grain boundaries and dimple patterns at all the test temperatures. In contrast, typical grain-boundary facets prevailed in specimens with straight grain boundaries.

References

1. M. YAMAZAKI, *J. Jpn Inst. Metals* **30** (1966) 1032.
2. M. KOBAYASHI, M. YAMAMOTO, O. MIYAGAWA, T. SAGA and D. FUJISHIRO, *Tetsu to Hagané* **58** (1972) 859.
3. M. YAMAMOTO, O. MIYAGAWA, M. KOBAYASHI and D. FUJISHIRO, *ibid.* **63** (1977) 1848.
4. H. KLEMM, *Metall.* **17** (1963) 113.
5. M. TANAKA, O. MIYAGAWA, T. SAKAKI and D. FUJISHIRO, *Tetsu to Hagané* **65** (1979) 939.
6. H. IIZUKA and M. TANAKA, *J. Mater. Sci.* **21** (1986) 2803.
7. M. TANAKA, H. IIZUKA and F. ASHIHARA, *ibid.* **23** (1988) to be published.
8. M. YOSHIBA, O. MIYAGAWA and D. FUJISHIRO, *Tetsu to Hagané* **68** (1982) 1813.
9. C. R. BROOKS, "Heat Treatment, Structure and Properties of Nonferrous Alloys" (American Society for Metals, Metals Park, Ohio, 1982) p. 394.
10. R. TANAKA, M. KIKUCHI, T. MATSUO, S. TAKEDA, N. NISHIKAWA, T. ICHIHARA and M. KAJIHARA, in Proceedings of the Fourth International Symposium on Superalloys, Seven Springs Mountain Resort, Champion, Pennsylvania, edited by J. K. Tien, S. T. Wlodek, H. Morrow III, M. Gel and G. E. Maurer (American Society for Metals, Metals Park, Ohio, 1980) p. 481.
11. N. YUKAWA and K. SATO, *Trans. Jpn Inst. Metals* **9** (1968) 680.
12. C. T. SIMS and W. C. HAGEL, "The Superalloys" (Wiley, New York, 1972) pp. 55, 153.
13. C. T. SIMS, N. S. STOLOFF and W. C. HAGEL, "Superalloys II" (Wiley, New York, 1987) pp. 115, 146.
14. K. N. TU and D. TURNBULL, *Acta Metall.* **15** (1967) 369.
15. M. TANAKA, O. MIYAGAWA and D. FUJISHIRO, *J. Jpn Inst. Metals* **38** (1974) 899.

Received 3 May
and accepted 9 September 1988